

# PRMT5 promotes full-length *HTT* expression by repressing multiple proximal intronic polyadenylation sites

Manisha Yadav<sup>1,2,†</sup>, Mona A. AlQazzaz<sup>3,†</sup>, Felipe E. Ciamponi<sup>4,†</sup>, Jolene C. Ho<sup>3</sup>, Maxim I. Maron<sup>5</sup>, Aiden M. Sababi<sup>6,7</sup>, Graham MacLeod<sup>6</sup>, Moloud Ahmadi<sup>8</sup>, Garrett Bullivant<sup>9</sup>, Vincent Tano<sup>10</sup>, Sarah R. Langley<sup>10,11</sup>, María Sánchez-Osuna<sup>12</sup>, Patty Sachamitr<sup>9</sup>, Michelle Kushida<sup>9</sup>, Costanza Ferrari Bardile<sup>13</sup>, Mahmoud A. Pouladi<sup>13</sup>, Rebecca Kurtz<sup>14</sup>, Laura Richards<sup>1,2</sup>, Trevor Pugh<sup>1,2,15</sup>, Mike Tyers<sup>12</sup>, Stephane Angers<sup>6,8</sup>, Peter B. Dirks<sup>9,16,17</sup>, Gary D. Bader<sup>1,2,6,7,18,19</sup>, Ray Truant<sup>14</sup>, Katlin B. Massirer<sup>4</sup>, Dalia Barsyte-Lovejoy<sup>3,20</sup>, David Shechter<sup>5</sup>, Rachel J. Harding<sup>3,8,20,\*</sup>, Cheryl H. Arrowsmith<sup>1,2,3,\*</sup>, Panagiotis Prinos<sup>3,\*</sup>

<sup>1</sup>Department of Medical Biophysics, University of Toronto, Toronto, ON, M5G1L7, Canada

<sup>2</sup>Princess Margaret Cancer Centre, University Health Network, Toronto, ON, M5G1L7, Canada

<sup>3</sup>Structural Genomics Consortium, University of Toronto, Toronto, ON, M5G1L7, Canada

<sup>4</sup>Center for Molecular Biology and Genetic Engineering, University of Campinas (UNICAMP), Campinas 13083-872, Brazil

<sup>5</sup>Department of Biochemistry, Albert Einstein College of Medicine, Bronx, NY 10461, United States

<sup>6</sup>Donnelly Centre for Cellular and Biomolecular Research, University of Toronto, Toronto, ON, M5S3E1, Canada

<sup>7</sup>Department of Molecular Genetics, University of Toronto, Toronto, ON, M5S3E1, Canada

<sup>8</sup>Leslie Dan Faculty of Pharmacy, University of Toronto, Toronto, ON, M5S3M2, Canada

<sup>9</sup>Developmental and Stem Cell Biology Program and Arthur and Sonia Labatt Brain Tumor Research Centre, The Hospital for Sick Children, Toronto, ON, M5G0A4, Canada

<sup>10</sup>Lee Kong Chian School of Medicine, Nanyang Technological University, 636921, Singapore

<sup>11</sup>School of Biosciences, Cardiff University, Cardiff CF103AX, United Kingdom

<sup>12</sup>Institute for Research in Immunology and Cancer, Université de Montréal, Montreal, QC, H3C3J7, Canada

<sup>13</sup>Department of Medical Genetics, Centre for Molecular Medicine and Therapeutics, Djavad Mowafaghian Centre for Brain Health, British Columbia Children's Hospital Research Institute, University of British Columbia, Vancouver, BC V5Z4H4, Canada

<sup>14</sup>Department of Biochemistry and Biomedical Sciences, McMaster University, Hamilton, ON L8N3Z5, Canada

<sup>15</sup>Ontario Institute for Cancer Research, University Health Network, Toronto, ON, M5G0A3, Canada

<sup>16</sup>Division of Neurosurgery, Department of Surgery, University of Toronto, Toronto, ON, M5S1A8, Canada

<sup>17</sup>Department of Laboratory Medicine and Pathobiology, University of Toronto, Toronto, ON M5S1A8, Canada

<sup>18</sup>Lunenfeld-Tanenbaum Research Institute, Sinai Health System, Toronto, ON, M5G1X5, Canada

<sup>19</sup>Department of Computer Science, University of Toronto, ON, M5S3E1, Canada

<sup>20</sup>Department of Pharmacology and Toxicology, University of Toronto, Toronto, ON, M5G1L7, Canada

\*To whom correspondence should be addressed. Email: takis.prinos@utoronto.ca

Correspondence may also be addressed to Rachel Harding. Email: rachel.harding@utoronto.ca

Correspondence may also be addressed to Cheryl H. Arrowsmith. Email: Cheryl.Arrowsmith@uhn.ca

†The first three authors should be regarded as Joint First Authors.

## Abstract

Expansion of the CAG trinucleotide repeat tract in exon 1 of the *Huntingtin* (*HTT*) gene causes Huntington's disease (HD) through the expression of a polyglutamine-expanded form of the HTT protein. This mutation triggers cellular and biochemical pathologies, leading to cognitive, motor, and psychiatric symptoms in HD patients. Targeting *HTT* splicing with small molecule drugs is a compelling approach to lowering HTT protein levels to treat HD, and splice modulators are currently being tested in the clinic. Here, we identify PRMT5 as a novel regulator of *HTT* messenger RNA (mRNA) splicing and alternative polyadenylation. PRMT5 inhibition disrupts the splicing of *HTT* introns 9 and 10, leading to the activation of multiple proximal intronic polyadenylation sites within these introns and promoting premature termination, cleavage, and polyadenylation of the *HTT* mRNA. This suggests that HTT protein levels may be lowered due to this mechanism. We also detected increasing levels of these truncated *HTT* transcripts across a series of neuronal differentiation samples, which correlated with lower PRMT5 expression. Notably, PRMT5 inhibition in glioblastoma stem cells potentially induced neuronal differentiation. We posit that PRMT5-mediated regulation of intronic polyadenylation, premature termination, and cleavage of the *HTT* mRNA modulates HTT expression and plays an important role during neuronal differentiation.

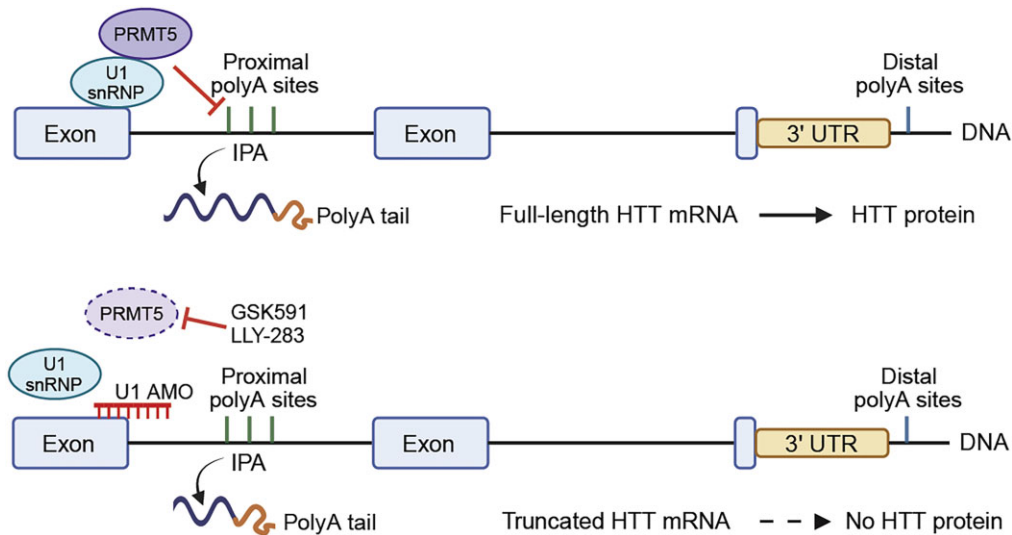
Received: May 6, 2024. Revised: April 7, 2025. Editorial Decision: April 8, 2025. Accepted: April 16, 2025

© The Author(s) 2025. Published by Oxford University Press on behalf of Nucleic Acids Research.

This is an Open Access article distributed under the terms of the Creative Commons Attribution-NonCommercial License

(https://creativecommons.org/licenses/by-nc/4.0/), which permits non-commercial re-use, distribution, and reproduction in any medium, provided the original work is properly cited. For commercial re-use, please contact reprints@oup.com for reprints and translation rights for reprints. All other permissions can be obtained through our RightsLink service via the Permissions link on the article page on our site—for further information please contact journals.permissions@oup.com.

## Graphical abstract



## Introduction

Huntington's disease (HD) is an autosomal dominant neurodegenerative disease that displays a range of psychiatric, cognitive, and physical symptoms [1], affecting ~1 in 10,000 people [2]. Characterized by the progressive loss of striatal neurons [3], HD is caused by the expansion of the CAG trinucleotide repeat tract in exon 1 of the *Huntingtin* (*HTT*) gene beyond a threshold of ~36 repeats, leading to the expression of a polyglutamine-expanded form of the HTT protein. Deletion of *Htt* is embryonically lethal in mice [4], and the protein is known to play important roles in numerous cellular processes critical for neuronal development [5]. The *HTT* locus spans 167 kb, encompassing 67 exons and 66 introns; thus, accurate RNA splicing regulation is essential for producing the mature and functional HTT protein. In the context of HD, the expression of a CAG-expanded but truncated form of *HTT* (*HTT1a*), generated by aberrant splicing, leads to the accumulation of a short polyadenylated messenger RNA (mRNA), which is translated to produce the toxic exon 1 protein fragment [4]. Other groups have reported a variety of *HTT* isoforms produced by alternative splicing [6–12]. More recently, splicing modulation has emerged as a promising therapeutic approach for lowering levels of HTT, a strategy currently being tested in clinical trials to slow or halt HD progression [13, 14]. The small-molecule splicing modulators, Branaplam and PTC-518, promote the inclusion of a poison pseudoexon within intron 49 in the *HTT* transcript, leading to the introduction of premature termination codons and nonsense-mediated decay (NMD) of the *HTT* mRNA, ultimately resulting in the lowering of HTT protein levels [6–8]. Nevertheless, the endogenous factors that regulate *HTT* splicing in normal physiology and development remain largely unknown.

Protein arginine methyltransferase 5 (PRMT5) catalyzes the symmetric dimethylation of arginine residues on target proteins, including histones, RNA-binding proteins, splicing factors, transcription factors and their complexes, DNA damage and repair factors, and metabolic regulators. Major PRMT5 cellular substrates include the spliceosomal Sm proteins SmD1 (SNRPD1), SmD3 (SNRPD3), and SmB/B'

(SNRNPB) [9–11]. Symmetric arginine methylation of these snRNP proteins is required for their efficient binding to the SMN protein and assembly into the mature spliceosome [10]. We and others have demonstrated the importance of PRMT5 for the maintenance of RNA splicing fidelity [12, 15–18]. PRMT5 inhibition results in widespread intron retention, leading to global downregulation of proteins implicated in cell proliferation [15, 17]. Interestingly, both PRMT5 and HTT are essential for neuronal stem cell proliferation and self-renewal [12, 19, 20]. Since splicing and RNA metabolism have been shown to play a central role in neurogenesis, neuronal differentiation, and neurodegenerative diseases [21–26], it is plausible that PRMT5 may regulate these processes via RNA splicing and that this role may intersect with HTT.

We previously identified PRMT5 as a regulator of splicing and stemness in glioblastoma (GBM) stem cells, and found that hundreds of intron retention events were the most prominent effect of PRMT5 inhibition on splicing [17]. Global proteome surveys linked the mis-splicing induced by PRMT5 inhibition to a global reduction of proteins involved in cell proliferation. Inspired by this and the recent discoveries of splicing modulators as HTT-lowering agents, we investigated the effects of PRMT5 inhibition on *HTT* mRNA splicing. Here, we show that PRMT5 inhibition impairs the splicing of *HTT* introns 9 and 10, leading to the activation of a cluster of cryptic alternative polyadenylation (APA) sites within these introns, resulting in premature cleavage and polyadenylation (PCPA) of the *HTT* mRNA and reduction of total HTT protein levels. Strikingly, we found increased levels of this truncated *HTT* isoform during neuronal differentiation, concomitant with lower PRMT5 levels, suggesting a physiological role for this regulation.

## Materials and methods

## Cell culture

Immortalized control and HD patient-derived fibroblasts were a kind gift from Professor Ray Truant and have been previously described [27]. TruHD Q43Q17, TruHD Q50Q40, TruHD Q57Q17, and TruHD Q66Q16 were derived from

HD patients, while TruHD Q21Q17 was derived from a control subject. These cells were cultured in Dulbecco's modified Eagle medium (DMEM) (Life Technologies #10370) with 15% (v/v) fetal bovine serum (FBS; Life Technologies), 1× GlutaMAX (Life Technologies #35050), and 1× penicillin streptomycin antibiotics. Cells were grown at 37°C with 5% CO<sub>2</sub>.

G523, G411, and G561 GBM cell lines were grown and maintained as previously described [17, 28]. GBM cells were grown in serum-free Neurocult NS-A Basal Medium (Stem Cell Technologies #05750) that is supplemented with 2 mM L-glutamine (Wisent #609-65-EL), 75 µg/ml Bovine Serum Albumin [BSA] (Life Technologies #15260-037), B27 supplement (Life Technologies #17504-44), rhEGF (10 ng/ml, Stem Cell Technologies #E9644), bFGF (10 ng/ml, Stem Cell Technologies #02634), N2-hormone mix (Thermo Fisher), and 2 µg/ml heparin sulfate (Sigma #H3149). Upon reaching confluence, cells were dissociated via mechanical trituration or with Accutase (Sigma, A6964) and re-plated on 10 cm plates (Corning) pre-coated with poly-L-ornithine (Sigma #P4957, 20 min) and laminin (Sigma #L2020).

### Treatment with PRMT5 inhibitors and control compounds

GBM, control, and HD patient fibroblasts were treated with PRMT5 inhibitors in six-well plates (Costar 6-well Clear TC-treated Multiple Well Plates, Corning) unless stated otherwise. Culture media was refreshed every 2 to 3 days with × 1 treatment.

Control and HD patient fibroblasts were plated in 384-well plates (Corning) at a density of 1000 cells/well, with four technical replicates per dose, and cultured across 10 dilution series (ranging from 1 nM to 10 µM) of PRMT5 inhibitors for 7 days. The effects of PRMT5 inhibitors on fibroblast cell viability were measured using CellTiter-Glo luminescent cell viability assay reagent (Promega, catalogue number: G7570). Cells were grown in 60 µl media. At the endpoint, plates were left to equilibrate to room temperature for 20 min, then 25 µl of CellTiter-Glo reagent was added to each well and mixed for a further 30 min protected from light. The luminescent signal intensity was subsequently read on a CLARIOstar plate reader (BMG LABTECH). Cell viability values were normalized to that of the dimethyl sulfoxide (DMSO)-treated controls for each line. Each data point was plotted using three independent biological replicates.

### Protein extraction and western blot

Lysis buffer containing 20 mM Tris-HCl (pH 8), 0.1% Triton X-100, 150 mM NaCl, 1 mM EDTA, 10 mM MgCl<sub>2</sub>, 1% SDS, protease inhibitor cocktail (in-house), and benzonase (in-house) was used to harvest total protein for western blot. Lysis buffer was added directly to cells on the plate and an aliquot was obtained to determine protein concentration using the Pierce™ BCA Protein Assay Kit (Catalog number: 23225). For all western blots, 15–35 µg of protein was loaded on NuPAGE 4%–12% Bis-Tris protein mini gels (catalog number NP0321BOX) and transferred onto polyvinylidene difluoride (PVDF) membranes. Primary antibodies used were anti-HTT (Abcam, #EPR5526, 1:1000; CST D7F7 #5656, 1:1000), anti-vinculin Antibody 7F9 (Santa Cruz, #sc-73614), anti-GAPDH (EMD Millipore, MAB374, 1:5000), anti-PRMT5 (Abcam, #EPR5772-ab109451, 1:1000), and

anti-β-Actin (5:10000; Santa Cruz sc-47778). Secondary antibodies used were IRDye® 680RD anti-mouse IgG (LI-COR, 926-68072, 1:5000) and IRDye® 800CW anti-rabbit IgG (LI-COR, 926-32211, 1:5000). Each western blot was replicated in at least three independent experiments. Membranes were visualized on an Odyssey® CLx Imaging System (LI-COR). Full, uncropped images of the western blots are shown in the source data file.

### PRMT5 knockdown using siRNAs

siRNAs for PRMT5 knockdown were purchased from Horizon Discovery (SMARTPool, 5 nM) and negative control siRNAs were purchased from Sigma (#SIC001-5 × 1NMOL). G523 GBM cells at 80% confluency were transfected with 5 µl siRNAs (stock concentration; 20 µM) in 2 ml media using TransIT-TKO transfection reagent.

### Allele separation western blot

To quantify and compare levels of full-length wild-type (WT) HTT and mutant HTT, we optimized an allele-separating western blot from [29]. Fifteen to thirty-five micrograms of lysate were run on 3%–8% Tris-acetate gradient protein gels (Catalog #: EA03785BOX) for 24 h at 120 V at 4°C until the 250 kDa ladder band ran out of the gel. Cold running buffer was refreshed twice during the run (25 mM Tris base, 190 mM glycine, 3.5 mM SDS, and 10.7 mM β-mercaptoethanol). Protein was transferred onto a 0.2 µm PVDF membrane (Bio-Rad) using the NuPAGE transfer buffer (25 mM Bicine, 25 mM Bis-Tris, 1 mM EDTA, and 15% methanol) at 70 V for 2 h. Membrane was then blocked for 1 h with 5% skimmed milk in phosphate-buffered saline with 0.05% Tween 20 (PBST) at room temperature. Primary antibodies used were for mutant HTT MW1 (Milipore # MABN2427). Secondary antibody use and membrane visualization are the same as described above.

### RNA extraction and quantitative real-time polymerase chain reaction

Complementary DNA (cDNA) was generated using the iScript gDNA Clear cDNA Synthesis Kit (Bio-Rad) according to the manufacturer's protocol. Five hundred nanograms to 1 µg of total RNA was treated initially with DNase to eliminate any residual genomic DNA contamination and then incubated with iScript reverse transcription supermix to produce cDNA required for the subsequent steps. For all quantitative reverse transcription polymerase chain reactions (qRT-PCRs), a no reverse transcription (RT) control was included as per the manufacturer's recommendations to control for residual genomic DNA contamination in reactions.

A 5× dilution was then made by adding 80 µl of double-distilled water, and 2 µl of synthesized cDNA was used per reaction. During qRT-PCR, cDNA template and LUNA master mix (NEB) were added into white PCR reaction tubes and placed in a CFX Maestro (Bio-Rad). All experiments were performed in at least four technical replicates and data were obtained from three to four independent experiments. Primers were designed to measure fully spliced transcripts and intron-containing transcripts, and all primer sequences are provided in [Supplementary Table S1](#). For data analysis, the threshold cycle (Ct) values obtained during qRT-PCR were used to calculate the ΔCtΔCt of intron-containing transcripts relative to the geometric mean of the expression of housekeeping genes

GAPDH and U6. Relative RNA expression ( $\Delta\Delta C_t$ ) of intron-containing was calculated by comparing PRMT5 inhibitor treated versus DMSO-treated samples. Statistical comparison was calculated using two-way ANOVA with Dunnett's multiple comparisons test compared to the mean of DMSO-treated cells. Data were collected on a Bio-Rad CFX96 touch and analyzed by Bio-Rad CFX Manager (v3.1.1517.0823) and GraphPad Prism versions 8, 9, and 10.

### 3'-End qRT-PCR

cDNA was synthesized using the P7-t25-vn oligo-dT primer with the following sequence: 5'-CAAGCAGAAGACGGCA TACGAGATTTTTTTTTTTTTTTTTTTTTTTTTTTTTTTTTV-N-3'.

qPCR was performed using the PowerUp SYBR Green Master Mix (Applied Biosystems, Cat. #A25742) on the CFX96 Touch Real-Time PCR Detection System (Bio-Rad), with the P7 primer and 5'-3' oligonucleotide sequences listed in [Supplementary Table S1](#).

### Proteomics analysis

Mass-spectrometry (MS) analysis was carried out as described previously [17]. Briefly, GSC lines G561, G564, and G583 were treated for 6 days either with 1  $\mu$ M of GSK591, 1  $\mu$ M LLY-283, or the inactive control, SGC2096 ( $n = 3$ ). Proteins were then extracted with denaturing urea buffer in the presence of protease and phosphatase inhibitors and digested with trypsin. Desalted peptides were analyzed by MS, "1D separation" on the Orbitrap Fusion instrument using liquid chromatography (LC) gradients. Peptide identification and label-free quantification were done in PEAKS (version X), considering relative abundance of all identified peptides for each protein. Subsequent data analysis was done in R (version 4.2.3). The MS proteomics data have been deposited to the ProteomeXchange Consortium (<http://proteomecentral.proteomexchange.org>) and are accessible via the PRIDE partner repository with the dataset identifier PXD021635 [17].

### Splicing data analysis

Intron retention data in the *HTT* gene presented as sashimi plots were extracted from bulk RNA-sequencing data from patient-derived GBM stem cells treated with 1  $\mu$ M GSK591 or SGC2096 as previously described [17]. We analyzed 297 published samples in total as follows: 139 samples from human induced pluripotent stem cell (hiPSC) [30], 40 samples from human embryonic stem cell (hESC) [31], 83 samples from hPSC-derived, 35 samples from hiPSC [32], and 288 samples from hiPSC.

Each dataset was evaluated to identify intron retention events (measured in PSI, or percentage spliced in) and gene expression values (in TPM, or transcripts per million). We utilized the vast-tools suite to compute intron retention events and gene expression values for each sample. Subsequently, we compared the PSI levels of introns 9 and 10, as well as the gene expression levels, across various cell types and stages of differentiation to identify statistically significant alterations between these variables. Furthermore, we conducted a thorough analysis of the VASTdb tissue/cell-line database to determine reliable intron retention patterns for the specific events in a panel that accurately depicts different stages of neuronal development. We encountered a notable constraint in the quantity of reads collected in the exon-exon and/or exon-intron junctions of the *HTT* gene in certain instances. To address

this, we utilized the "vast-tools combine" module to merge replicates and samples from identical experimental settings to perform adequate statistical inferences. The post-processing data analysis and figure-generating stages were performed using custom Python 3.7 scripts, which can be obtained upon request.

The RNA-sequencing of the isoHD allelic differentiation series from Ooi *et al.* [33] and Tano *et al.* [34] was used to visualize the expression levels of PRMT5 and WDR77 as well as the introns of *HTT*. This set included embryonic stem cells (ESCs,  $n = 9$ ), neural progenitor cells (NPCs,  $n = 9$ ), and neurons (NEU,  $n = 12$ ). Briefly, gene-level differential expression was performed using DESeq2 [35]. Junction-level differences in intron 9–10 in *HTT* were tested using JunctionSeq [36] normalized to other detected junctions, including introns 59–60 and 64–65. To visualize, the gene and exon/intron counts from all samples were normalized using the variance stabilizing transform from DESeq2 [35] and plotted with the boxplots from ggplot2. Boxplots represent the median (line), the 25th and 75th percentiles (hinges), and 1.5 times the interquartile range (whiskers). As in Tano *et al.* [34], the ESCs and NPCs were generated and sequenced as one experiment and are directly comparable. The NEUs were generated and sequenced as a second experiment.

### APA analysis in PRMT5 inhibitor-treated GBM cells

We performed single-cell (sc)RNA-sequencing using the 10x Genomics technology in two patient-derived GBM cell lines, G549 and G561, treated with vehicle DMSO or 1  $\mu$ M LLY-283. We used the MAAPER software package to assign sequencing reads to the known, curated polyadenylation (PA) sites [37]. A minimum threshold of 20 reads was set for each polyA site (PAS), while gene filtering was applied for genes with at least 40 reads.

Then, we used the APALog [38] software package in pairwise mode to quantify the APA events. This enabled us to assess APA usage across all known PA sites within transcripts. Using APALog, we calculated the base 2 logarithm ( $\text{Log}_2$ ) of the fold change to evaluate the significance of differential usage between distal and proximal PA sites.

### U1 antisense morpholino oligonucleotide transfection

U1 antisense morpholino oligonucleotide (AMO) (sequence: 5'-GGTATCTCCCCTGCCAGGTAAGTAT-3') and control AMO (sequence: 5'-CCTCTTACCTCAGTTACAATTTATA-3') were purchased from GeneTools, LLC. Endo-Porter PEG reagent, also purchased from GeneTools, LLC, was used for AMO transfection. Cells were seeded in six-well plates at 80% confluency. A 7.5  $\mu$ M concentration of either U1 or control AMOs was mixed with fresh media containing 10%–15% serum and Endo-Porter reagent at a concentration of 6  $\mu$ M. Cells were incubated for 3 days, with fresh media containing the respective AMOs replenished one day prior to cell collection.

### Neuronal differentiation reporter assays

To generate reporters for induction of neuronal lineage differentiation, we used CRISPR–Cas9 genome editing to insert an H2B-CITRINE coding sequence immediately into the *TUBB3*, *MAPT* (Tau), and *DCX* loci at the transcription start site (TSS) of the human GBM stem cell line G523. G523–CITRINE re-

porter cells were seeded in poly-L-ornithine + laminin-coated dishes and treated with either 1  $\mu$ M GSK591, 1  $\mu$ M LLY283, or 0.1% DMSO for 14 days with regular media changes. At 3, 10, and 14 days of treatment, cells were collected and fixed in 1% paraformaldehyde. Flow cytometry on fixed cells was performed using either a CytoFlex S or CytoFlex LS system (Beckman Coulter) using Fixable Viability Dye eFluor™ 660 (eBioscience) to gate for cell viability. Analysis was performed using CytExpert version 2.6 software (Beckman Coulter). Percentage of CITRINE-positive cells was determined based on gating in WT G523 cells (no reporter). All experiments were performed in triplicate.

## Results

### PRMT5 inhibition decreases *HTT* mRNA and protein levels in GBM models

We previously reported that PRMT5 inhibition impaired splicing and stemness in a large panel of patient-derived GBM stem cells. RNA-sequencing of GBM stem cells treated with 1  $\mu$ M GSK591, a potent and selective PRMT5 inhibitor, revealed widespread mis-splicing, with intron retention events being the most prevalent splicing alteration observed. One of the top affected genes in this study was *HTT* (Fig. 1A), which was significantly downregulated following PRMT5 inhibition with GSK591 in these lines. Proteomics analysis in three different patient-derived GBM cell lines (G561, G564, and G583) also showed decreased *HTT* protein levels following PRMT5 inhibition with 1  $\mu$ M GSK591 or LLY-283 (Fig. 1A). Building on this finding, we validated *HTT* mRNA downregulation by RT-qPCR, referred herein as qPCR, in three different GBM stem cell lines (Fig. 1B). The levels of *HTT* mRNA were significantly lower after treatment of GBM cells with either 1  $\mu$ M GSK591 or LLY-283 (Fig. 1B), both PRMT5 inhibitors, but not with an inactive control compound, SGC2096, a close chemical analog of the GSK591 chemical probe that is inactive up to 10  $\mu$ M against PRMT5 [39] (<https://www.thesgc.org/chemical-probes/gsk591>). Western blots of cell lysates from two patient-derived GBM lines treated with these compounds showed a consistent decrease in *HTT* protein following PRMT5 inhibition, corroborating the mRNA decrease with either GSK591 or LLY-283 (Fig. 1C and D, uncropped western blot images in [Supplementary Fig. S1](#)). Both inhibitors reduced the symmetric dimethyl-arginine levels, as assessed by western blots using a pan-SDMA antibody ([Supplementary Fig. S2](#)). This reduction in *HTT* mRNA and protein was also corroborated with siRNA-mediated knockdown of PRMT5, though to a lesser degree compared to chemical inhibition ([Supplementary Fig. S3](#)).

### PRMT5 inhibition lowers *HTT* mRNA and protein levels in control and HD fibroblasts

Prompted by these findings, we next asked whether this phenomenon could also be observed in cell models of HD. We used h-TERT-immortalized control and HD patient-derived fibroblast lines [27], with *HTT* gene CAG repeat tracts between 40 and 50, close to the most common clinically observed range. PRMT5 inhibition with either 1  $\mu$ M GSK591 or LLY-283 in these lines resulted in a ~50% decrease of *HTT* mRNA compared to DMSO-treated cells (Fig. 2A), paralleling what we observed in GBM cells. Western blot analysis showed a consistent reduction in *HTT* protein levels across the se-

ries of fibroblast lines tested, including a homozygous HD line (Q50Q40), a heterozygous WT line (Q21Q18), and three heterozygous HD lines (Q43Q17, Q57Q17, and Q66Q16) (Fig. 2B and C, uncropped western blots shown in [Supplementary Fig. S4](#)). Similar to our previous observations in GBM cell lines [17], LLY-283 produced a larger reduction in *HTT* protein levels than GSK591 (Fig. 2B and D), consistent with greater potency of LLY-283 over GSK591 for inhibition [17]. Titration of LLY-283 in this cell line showed that significant *HTT* lowering was evident at 10 nM and peaked at 100 nM (Fig. 2C; full western blots shown in [Supplementary Fig. S4](#)), closely following the potency of the compound for *in-cell* target inhibition [40]. Cell viability was not significantly affected at any dose of LLY-283 up to 1  $\mu$ M, indicating that the observed *HTT* lowering is not an artifact of cell death. To investigate whether the expanded allele of *HTT* was affected differently than the WT, we analyzed cell lysates using an allele separation western blot and the anti-polyglutamine antibody, MW1 [29, 41]. This revealed that the PRMT5 inhibitor treatment led to a total *HTT* lowering, with approximately equal decreases in both WT and expanded *HTT* levels (Fig. 2E; uncropped western blots shown in [Supplementary Fig. S5](#)).

### PRMT5 inhibition activates multiple cryptic intronic PAS leading to PCPA of *HTT* mRNA

Our previous study showed that PRMT5 inhibitor treatment induces widespread mis-splicing in GBM cells. Therefore, we reasoned that changes to *HTT* splicing could be the mechanism by which *HTT* mRNA and protein levels are lowered by PRMT5 inhibition. Data mining of our bulk GBM RNA-seq data revealed that two introns [7, 8] of *HTT* were mis-spliced upon PRMT5 inhibition, with inclusion levels prominently increased in GBM cells treated with PRMT5 inhibitors (Fig. 3A). The remaining introns of the *HTT* gene analyzed were unaffected (for example, intron 39 and Fig. 3B). Experimental validation of intron retention by qPCR showed dramatic and significant increases for both introns 9 and 10 following PRMT5 inhibition in GBM cells (Fig. 3C and D), compared to control introns (Fig. 3E). Visual inspection of the read density across introns 9 and 10 revealed that the intronic reads were diminishing toward the second half of intron 10 (Fig. 3A). Intriguingly, we found the same trend when analyzing RNA-seq data from A549 lung cancer cells treated with GSK591 ([Supplementary Fig. S6](#)) from another study that investigated the effect of PRMT5 inhibitors on intron retention [16]. The nature and consistency of the RNA-seq reads across these two *HTT* introns suggested transcription termination occurring in the distal part of intron 10. In support of this premise, there was a visible decrease in exonic reads after exon 10 in GSK591-treated GBM and A549 cells (Fig. 3B and [Supplementary Fig. S6](#)). These observations suggested that PRMT5 inhibition may result in transcriptional read decrease, consistent with increased RNA polymerase termination or pausing in that intron. A likely explanation for this observation is the activation of intronic PAS, leading to PCPA of the *HTT* mRNA.

To further explore PCPA as a possible mechanism of PRMT5 inhibitor-induced *HTT* lowering, visual inspection of the sequences of *HTT* introns 9 and 10 revealed six potential APA motifs: four clustered toward the distal part of intron 10 (labeled 10A–D in Fig. 4A) and two in intron 9 (labeled 9A and B, Fig. 4E). We designed qPCR primers upstream of these

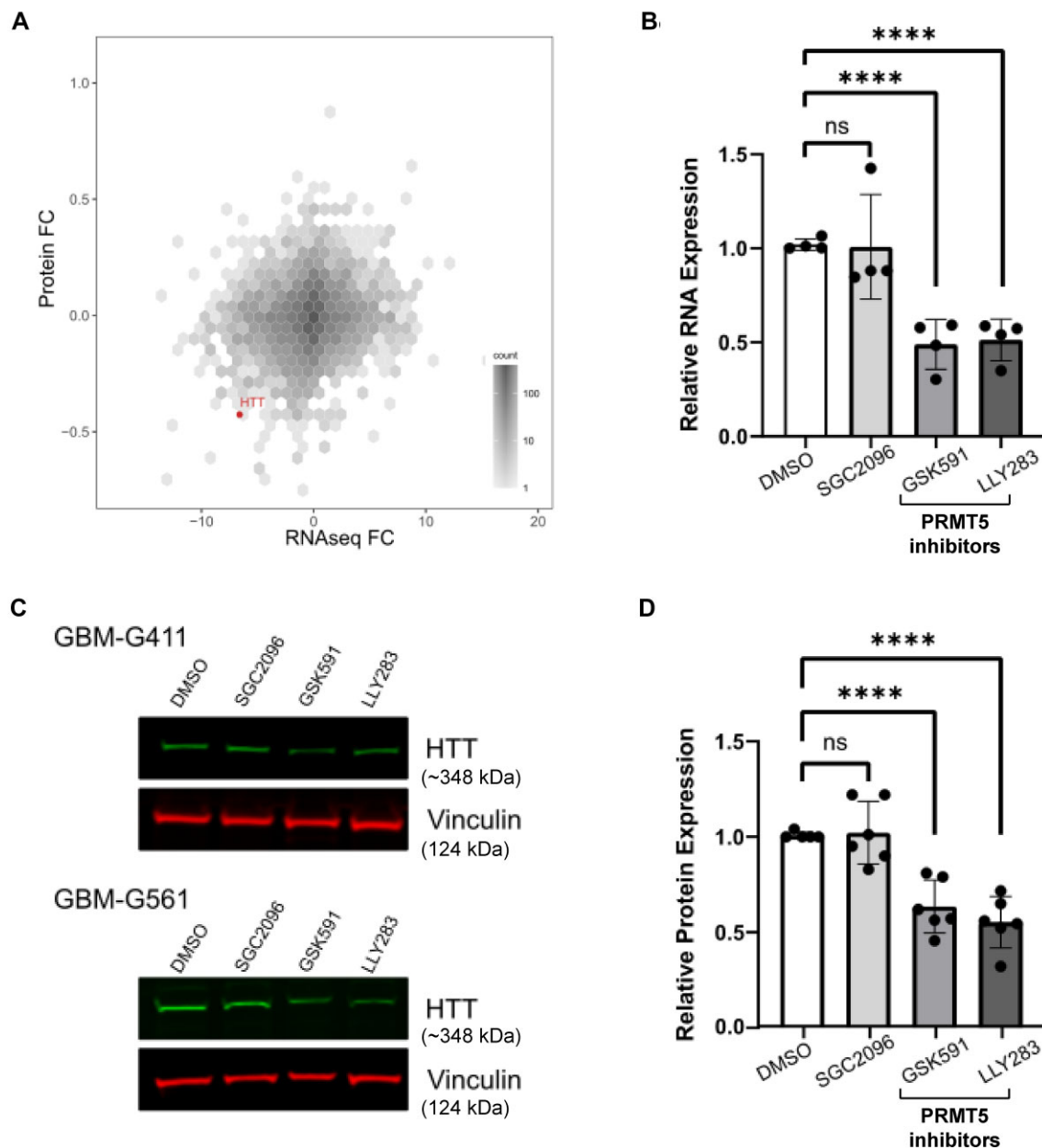


**Figure 1.** PRMT5 inhibitor treatment in GBM cell lines causes lowering of HTT protein and RNA. **(A)** Integration of RNA-sequencing and proteomics analysis following PRMT5 inhibition in three independent patient-derived GBM lines showing HTT protein and RNA levels are both reduced with PRMT5 inhibitors GSK591 and LLY283. The graph represents average fold change ( $\log_2$ ) after PRMT5 inhibition, combining all three G561, G564, and G583 cell lines and both PRMT5 inhibitors, GSK591 and LLY283, against SGC2096 (negative control) ( $n = 3$ ). Gene density is represented by color intensity ("counts,"  $\log_{10}$ ). **(B)** RT-qPCR analysis of patient-derived GBM cell lines treated with DMSO, 1  $\mu$ M SGC2096 (negative control), 1  $\mu$ M GSK591 (PRMT5 inhibitor), and 1  $\mu$ M LLY283 (PRMT5 inhibitor) for 5–7 days,  $n = 3$ –5 biological replicates of G523, G411, and G561. PRMT5 inhibitors resulted in a significant lowering of total HTT expression levels relative to DMSO-treated cells. Data are the mean  $\pm$  standard error of the mean (SEM) of four independent biological replicates, each comprising four technical replicates. Statistical significance was calculated using two-way ANOVA with Dunnett's multiple comparisons test compared to the mean of DMSO-treated cells. ns: not significant  $P$  value = .997, \*\*\*\* $P$  value < .0001. **(C)** Representative western blots of G411 and G561 showing significant lowering of HTT protein levels upon treatment with 1  $\mu$ M GSK591 or 1  $\mu$ M LLY283. The full blots are shown in [Supplementary Fig. S1](#). **(D)** Western blot quantification is shown as a bar graph. HTT protein levels were normalized to vinculin and plotted relative to levels observed with DMSO control treatment. Data are the mean  $\pm$  SEM of four independent biological replicates of G523, G411, and G561. Statistical significance was calculated using two-way ANOVA with Dunnett's multiple comparisons test compared to the mean of DMSO-treated cells. ns  $P$  value = .921, \*\*\*\* $P$  value < .0001.

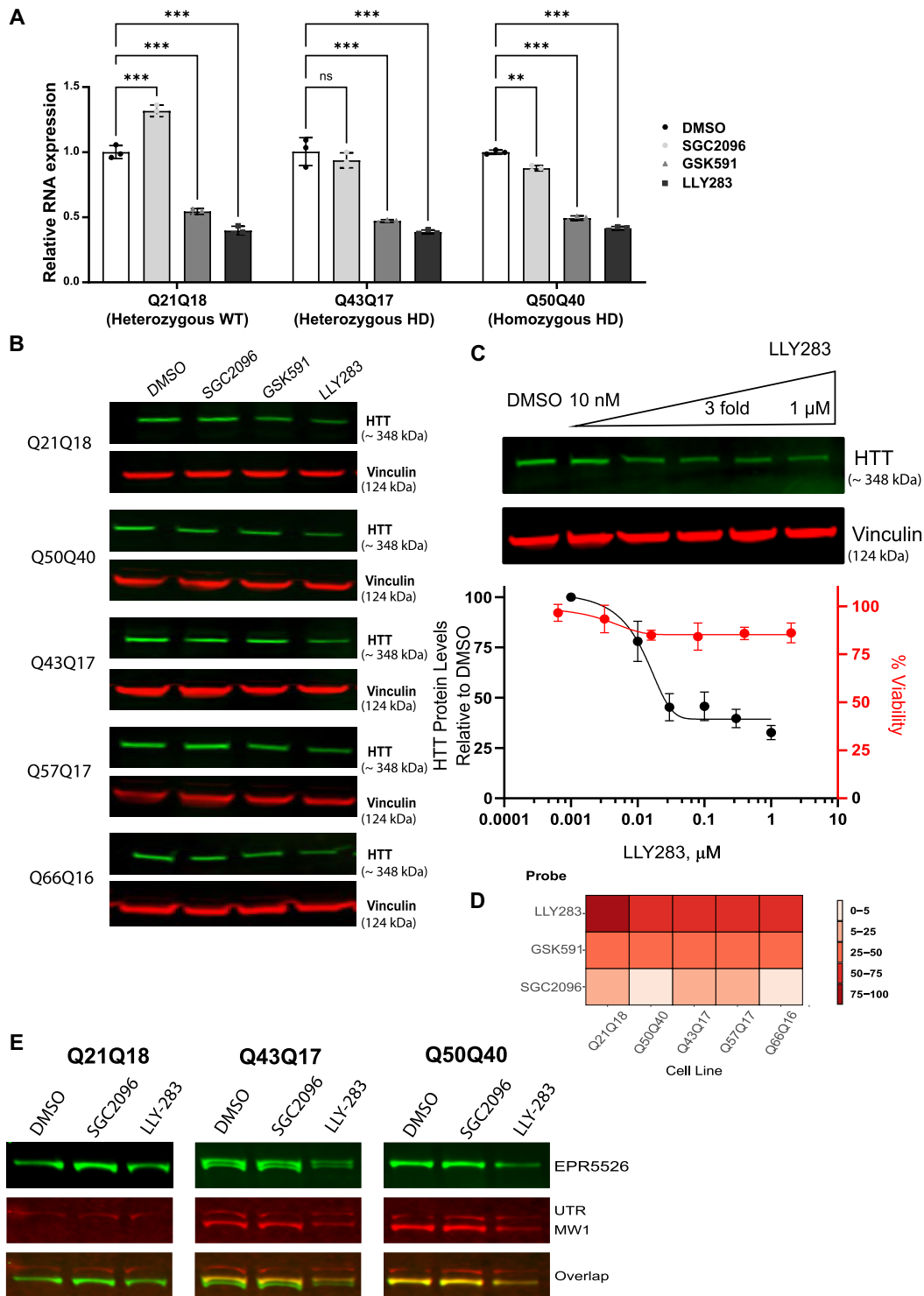


**Figure 2.** PRMT5 inhibitors lower HTT in control and HD fibroblasts at both the RNA and protein level. **(A)** Barplot showing relative *HTT* mRNA expression by RT-qPCR analysis in the indicated TruHD fibroblast cell lines treated with DMSO, 1 μM SGC2096 (negative control), 1 μM GSK591 (PRMT5 inhibitor), and 1 μM LLY283 (PRMT5 inhibitor) for 5 days. Data were analyzed using two-way ANOVA. Data are shown as mean ± standard deviation (sd);  $n = 3$  technical replicates. \*\*\* $P < .001$ , \*\* $P < .01$ , \* $P < .05$ , ns: not significant. **(B)** Representative western blot of HTT and vinculin showing consistent HTT lowering upon treatment with 1 μM LLY283 in homozygous, (Q50Q40), heterozygous (Q43Q17, Q57Q17, and Q66Q16), and control (Q21Q18) fibroblasts. The uncropped western blots are shown in [Supplementary Fig. S4](#). **(C)** Top panel: western blot analysis of HTT and vinculin in control and HD fibroblasts after 5 days of treatment with LLY283 at different concentrations. See also [Supplementary Fig. S4](#). Bottom panel: cell viability study of Q43Q17 HD fibroblasts showing no cell death within the concentration range of LLY283 used in experiments. **(D)** Heatmap comparing the relative HTT protein lowering in HD (Q50Q40, Q43Q17, Q57Q17, and Q66Q16) and WT (Q21Q18) fibroblasts when treated with 1 μM PRMT5 inhibitors (LLY283 or GSK591) or negative control (SGC2096).  $N = 4-8$  biological replicates. **(E)** Representative western blot probed by antibody EPR5526 for total HTT protein levels and MW1 for mutant HTT levels in HD fibroblasts. PRMT5 inhibition lowered total HTT levels in HD fibroblasts expressing mutant HTT (Q50Q40, Q43Q17) and control fibroblasts expressing WT HTT (Q21Q18). Utrophin (UTRN) was used as a loading control. The full blots are shown in [Supplementary Fig. S5](#).

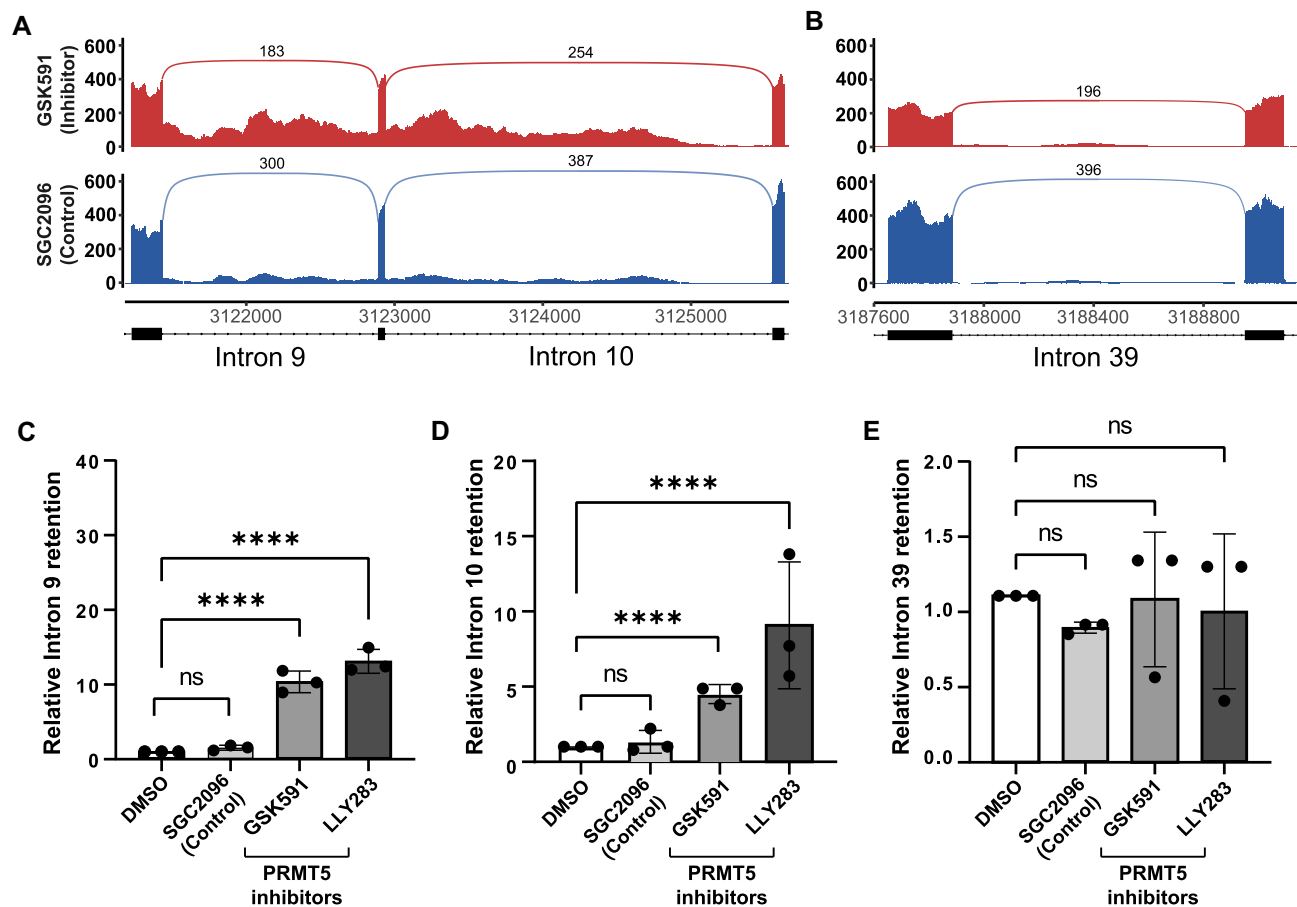


**Figure 3.** Increase in specific intronic sequences in the HTT transcript after PRMT5 chemical inhibition. **(A)** Intron retention data in the *HTT* gene presented as sashimi plots [62] were extracted from bulk RNA-seq data from patient-derived GBM stem cells treated with 1  $\mu$ M GSK591 or SGC2096 as described previously [17]. **(B)** Intron retention data for *HTT* intron 39 as a control. For both panels (A) and (B), x-axis represents the genomic coordinates along the chromosome and y-axis shows the normalized read count at each position. The lines with numbers connecting the individual exons represent the number of reads that map to the exon–exon junction. Bar plots showing the mean  $\pm$  SEM of three independent biological replicates, each comprising four technical replicates. Statistical significance was calculated using two-way ANOVA with Dunnett’s multiple comparisons test compared to the mean of DMSO-treated cells. *P* value  $\geq$  .05 is considered insignificant. \*\*\*\**P* value < .0001.

sites and performed qPCRs using total RNA from the GBM stem cell line G523. We used an oligo-dT primer bearing a P7 adapter for the RT step and the P7 adapter primer coupled to gene-specific primers for the PCR steps as highlighted in Fig. 4B [42]. We observed very prominent and significant induction of the intronic PAS sites in *HTT* intron 10 upon PRMT5 inhibition, compared to the canonical *HTT* PAS sites (Fig. 4C). Next, we queried the polyA-site database [43] for the presence of experimentally curated APA sites in the *HTT* gene and found the vast majority mapped within *HTT* intron 10, and were identical with the PAS we identified (Table 1). Finally, we used pseudo-bulk profiles from scRNA-seq data derived from GBM stem cells treated with LLY-283 to analyze PCPA in the *HTT* transcripts [26] (see the “Materials and methods” section). Strikingly, all of the identified major APA events mapped within *HTT* introns 9 and 10 (Fig. 4D and Table 1). One of the top-ranked sites by fold change and *P*-value mapped to intron 9 (labeled 9C in Fig. 4D and Table 1). To investigate further, we designed primers for that site (Fig. 4E) and performed qPCR using the same RT reaction described above. We observed prominent activation of the intron 9 distal PAS site, corresponding to the same site identified by scRNA-seq (Fig. 4F,

right panel). Additionally, we found two more proximal PAS sites in intron 10 (labeled 10E and F in Fig. 4D and Table 1), which we validated by qPCR (Fig. 4F, left panel). Intronic PA of the *HTT* transcript could potentially result in truncated *HTT* protein products. We investigated this possibility by analyzing cell lysates treated with LLY-283 or vehicle (DMSO) by western blotting. The complete sodium dodecyl sulfate–polyacrylamide gel electrophoresis (SDS–PAGE) was transferred and probed with the *HTT* antibody, EPR5526, which recognizes an N-terminal *HTT* peptide predicted to be retained in the truncated *HTT* isoform. The putative PRMT5i-induced truncated *HTT* protein product is predicted to retain the first 428 amino acids and have an additional 19 amino acids introduced by intronic sequences, resulting in a  $\sim$ 49 kDa N-terminal *HTT* fragment. We detected several low molecular weight N-terminal *HTT* fragments, but these were unchanged in the LLY-283-treated cells compared to the DMSO control (Supplementary Fig. S7). Moreover, we were unable to detect any additional lower molecular weight bands induced in the LLY-283-treated samples (Supplementary Fig. S7). We also tested a panel of *HTT* antibodies recognizing different *HTT* epitopes, which similarly did not reveal any additional bands

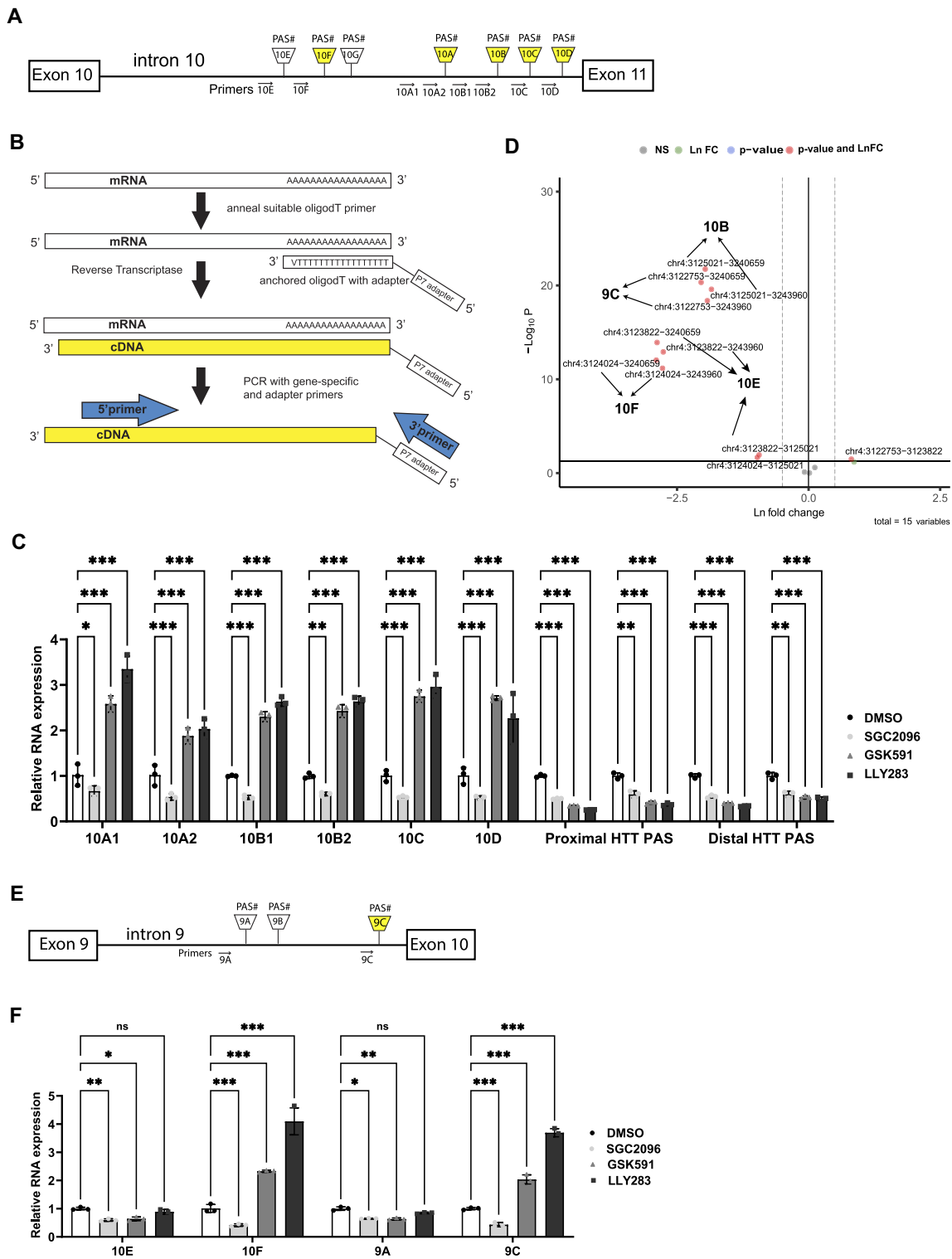


**Figure 4.** PRMT5 inhibition induces activation of APA sites in *HTT* introns 9 and 10. **(A)** Schematic of intron 10 APA sites detected in this study by visual scanning for polyA motifs and scRNA-seq data analysis. **(B)** Schematic of the RT-qPCR-based approach for the detection and validation of 3' cDNA ends. **(C)** RT-qPCR validation of the potential APA sites using RNA from GBM cells treated with the indicated compounds. For reference, we designed two primers specific for each of the 2 canonical *HTT* PAS sites (indicated as proximal and distal PAS). Data were analyzed using two-way ANOVA. Data are shown as mean  $\pm$  SD;  $n=3$  technical replicates. \*\*\* $P < .001$ , \*\* $P < .01$ , \* $P < .05$ , ns: not significant. **(D)** Volcano plot of APA events identified in *HTT* gene using scRNA-seq data from GBM cells treated with LLY-283 or DMSO for all the APA pairs between proximal and distal PA sites. Fifteen pairwise APA events were observed for the *HTT* gene. The  $x$ -axis denotes the natural logarithm (Ln) fold change of distal to proximal PAS utilization. Hence, the negative values indicate proximal PAS usage, and positive values indicate distal PAS usage. We see significant usage of intronic PA sites located in Intron 9 (chr4: 3 122 753) and 10 (chr4: 3 125 021) of the *HTT* gene for the LLY-283-treated cell lines compared to the controls. **(E)** Schematic of potential PAS sites mapping in *HTT* intron 9. Yellow indicates sites that have been experimentally validated. **(F)** RT-qPCR validation of *HTT* introns 9 and 10 (additional) PAS sites. Data were analyzed using two-way ANOVA. Data are shown as mean  $\pm$  SD;  $n=3$  technical replicates. Asterisks indicate statistical significance based on calculated  $P$ -values. \*\*\* $P < .001$ , \*\* $P < .01$ , \* $P < .05$ , ns: not significant.

**Table 1.** Coordinates of APA sites (PAS) in the *HTT* gene identified by scRNA-seq analysis of two patient-derived GBM lines treated with 1  $\mu$ M LLY-283 or DMSO

PAS name	PAS coordinates	Location	Primers	Experimentally validated	polyA_DB id
9A	Chr4: 3 121 764	Intron 9, 1st proximal PAS	#15 = 9A	No	NA
9B	Chr4: 3 121 776	Intron 9, 2nd proximal PAS		No	NA
9C	Chr4: 3 122 753	Intron 9, distal PAS	#16 = 9C	Yes	Chr4: 3 122 753
10A	Chr4: 312 727	Intron 10, 1st distal polyA motif	#3, #4 10A1, 10A2	Yes	NA
10B	Chr4: 3 125 021	Intron 10, 2nd distal polyA	#5, #6, 10B1, 10B2	Yes	Chr4: 3 125 021
10C	NA	Intron 10, 3rd distal polyA	#7 = 10C	Yes	NA
10D	Chr4: 3 125 289	Intron 10, 4th distal APA	#8 = 10D	Yes	Chr4: 3 125 289
10E	Chr4: 3 123 822	Intron 10, 1st proximal PAS	#13 = 10E	No	Chr4: 3 123 822
10F	Chr4: 3 123 953	Intron 10, 2nd proximal PAS	#14 = 10F	Yes	Chr4: 3 123 953
10G	Chr4: 3 124 024	Intron 10, 3rd proximal PAS	#14 = 10F	No	Chr4: 3 124 024

in the LLY-283-treated samples (Supplementary Fig. S8). In conclusion, these data collectively suggest the induction of PCPA within introns 9 and 10 of *HTT* following PRMT5 inhibition.

### Inhibition of U1 snRNA binding via an U1 AMO phenocopies PRMT5 inhibition and leads to PCPA of the *HTT* mRNA transcript

Previous evidence pointed to a role for the U1 snRNP in globally suppressing intronic PCPA, particularly in long neuronal genes such as *HTT* [44–46]. Given that PRMT5 methylates Sm proteins to facilitate spliceosome assembly, we reasoned that the mechanism of APA induction of the *HTT* mRNA by PRMT5 could be similar to U1 snRNP inhibition (outlined in schematic in Fig. 5A). We employed a previously described AMO to inhibit U1 snRNA binding in transfections of the patient-derived GBM stem cell line G523 and the commonly used GBM line U87 (see schematic in Fig. 5A). We observed increased levels of *HTT* transcripts retaining intron 9 and 10 sequences (Fig. 5B and Supplementary Fig. S9A) in both G523 and U87 GBM lines, similar to PRMT5 inhibitors GSK591 and LLY-283. Interestingly, intron 39 showed the reverse trend, i.e. lower levels with U1 AMO, consistent with lower RNA polymerase II elongation rates past *HTT* intron 10. This led to a global reduction in *HTT* mRNA levels (Fig. 5B and Supplementary Fig. S9A), similar to our observations with PRMT5 inhibitors. Strikingly, we observed activation of the same PAS sites in *HTT* introns 9 and 10 that we identified with PRMT5 inhibitors (Fig. 5D and Supplementary Fig. S9B). The PAS site in intron 9 was more prominent with the U1 AMO, suggesting that this site is more dominant when U1 snRNP is inhibited (Fig. 5D and Supplementary Fig. S9B). We observed the same trends in the WT (Q21Q18) fibroblast cell line (Fig. 5C and E), suggesting a conserved mechanism across cell types. These data indicate that PRMT5 and U1 snRNP suppress PCPA in introns 9 and 10 of the *HTT* mRNA.

### Increased expression of APA *HTT* isoforms during neuronal differentiation

We were able to detect truncated APA *HTT* isoforms with 3'UTRs composed of intron 9 and 10 sequences in the untreated control conditions in GBM cells, so we reasoned they are likely expressed in specific neuronal tissues. To investigate this possibility, we mined VastDB, an alternative splicing database containing a large compendium of vertebrate gene splice variants and their expression data across different human tissues [47]. Data mining revealed increased levels of

*HTT* transcripts with intron 9 and 10 sequences retained during early neuronal development (Supplementary Fig. S10A). Strikingly, PRMT5 expression showed the inverse trend, i.e. its expression was high in neural stem cells and NPCs but decreased drastically during early embryonic neuronal development (Supplementary Fig. S10B). Prompted by this, we mined publicly available neuronal RNA-seq datasets [30, 32, 48] for expression of *HTT* transcripts retaining these introns. We found higher levels of APA *HTT* transcripts with intron 9 and 10 sequences in differentiated neurons as compared to earlier, less differentiated cell types, represented by hiPSCs and NPCs (Fig. 6A). Interestingly, mixed neuron/astrocyte populations, which are indicative of inefficient or incomplete neuronal differentiation [49] did not show this increase (Fig. 6A). Concomitant with this increase in APA *HTT* transcripts bearing intron 9 and 10 sequences, we saw a significant decrease of PRMT5 expression in neurons compared to cells earlier in the "differentiation process (Fig. 6B). Decreased PRMT5 expression during neuronal differentiation was also observed by Braun *et al.* [15].

We also analyzed a series of isogenic iPSC-derived HD neuronal cell models [34, 33] and found a stepwise increase in APA *HTT* transcripts with intron 9 and 10 sequences during neuronal differentiation from hESCs to neurons (Supplementary Fig. S11A). In the same neuronal differentiation series, we found that the expression of PRMT5 and its cofactor WDR77 decreased during neuronal differentiation (Supplementary Fig. S11B). We conclude that the truncated APA *HTT* transcript isoforms bearing 3'UTRs with intron 9 and 10 sequences are increasingly prevalent through the course of neuronal differentiation and inversely correlate with PRMT5/WDR77 levels.

### PRMT5 inhibition induces neuronal differentiation in GBM stem cells

In order to ascertain the functional impact of PRMT5 downregulation in the differentiation capacity of GBM stem cells, we generated three different neuronal differentiation reporter assays by using CRISPR–Cas9 genome editing to insert an H2B-CITRINE coding sequence immediately into the TUB $\beta$ 3, Doublecortin (DCX), and MAPT loci at the TSS of the human GBM stem cell line G523. Fourteen-day treatment with 1  $\mu$ M GSK591 or LLY-283 induced a dramatic induction of the TUB $\beta$ 3, DCX-, and MAPT-Citrine reporters in these cells (Fig. 6C). This strongly suggests that PRMT5 activity is required to keep the cells cycling and undifferentiated. Thus, the decrease in PRMT5 expression we observed in neurons

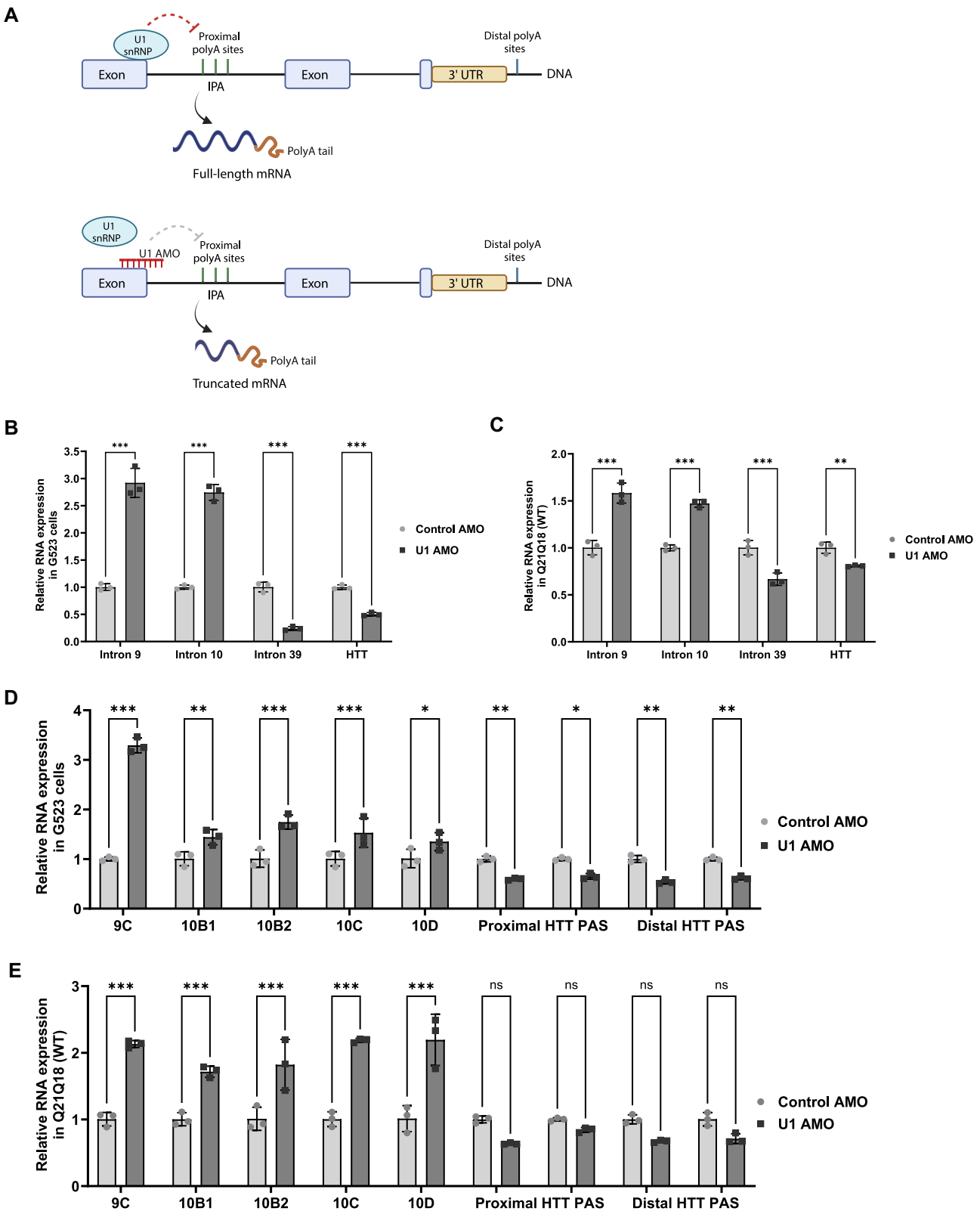


**Figure 5.** U1 snRNP inhibition results in PCPA in *HTT* introns 9 and 10. **(A)** Schematic depicting the effect of U1 snRNP in suppressing proximal intronic polyadenylation (IPA) leading to mRNA PCPA and the effect of U1 AMO in promoting IPA and PCPA. Created with BioRender.com (<https://BioRender.com/jknh0zu>). RT-qPCR validation with primers specific for the indicated *HTT* introns in G523 GBM **(B)** and WT Q21Q18 fibroblast **(C)** cells transfected with 7.5  $\mu$ M U1 AMO or control AMO for 3 days. Effect of U1 AMO on the intron 9 and 10 cryptic APA sites using RNA from G523 GBM **(D)** and Q21Q18 fibroblast **(E)** cells transfected with the U1 or control AMO. For reference, we used two primers specific for each of the two canonical *HTT* sites (indicated as proximal and distal PAS). Data were analyzed using two-way ANOVA. Data are shown as mean  $\pm$  SD;  $n=3$  technical replicates. Asterisks indicate statistical significance. \*\*\* $P < .001$ , \*\* $P < .01$ , \* $P < .05$ , ns: not significant.

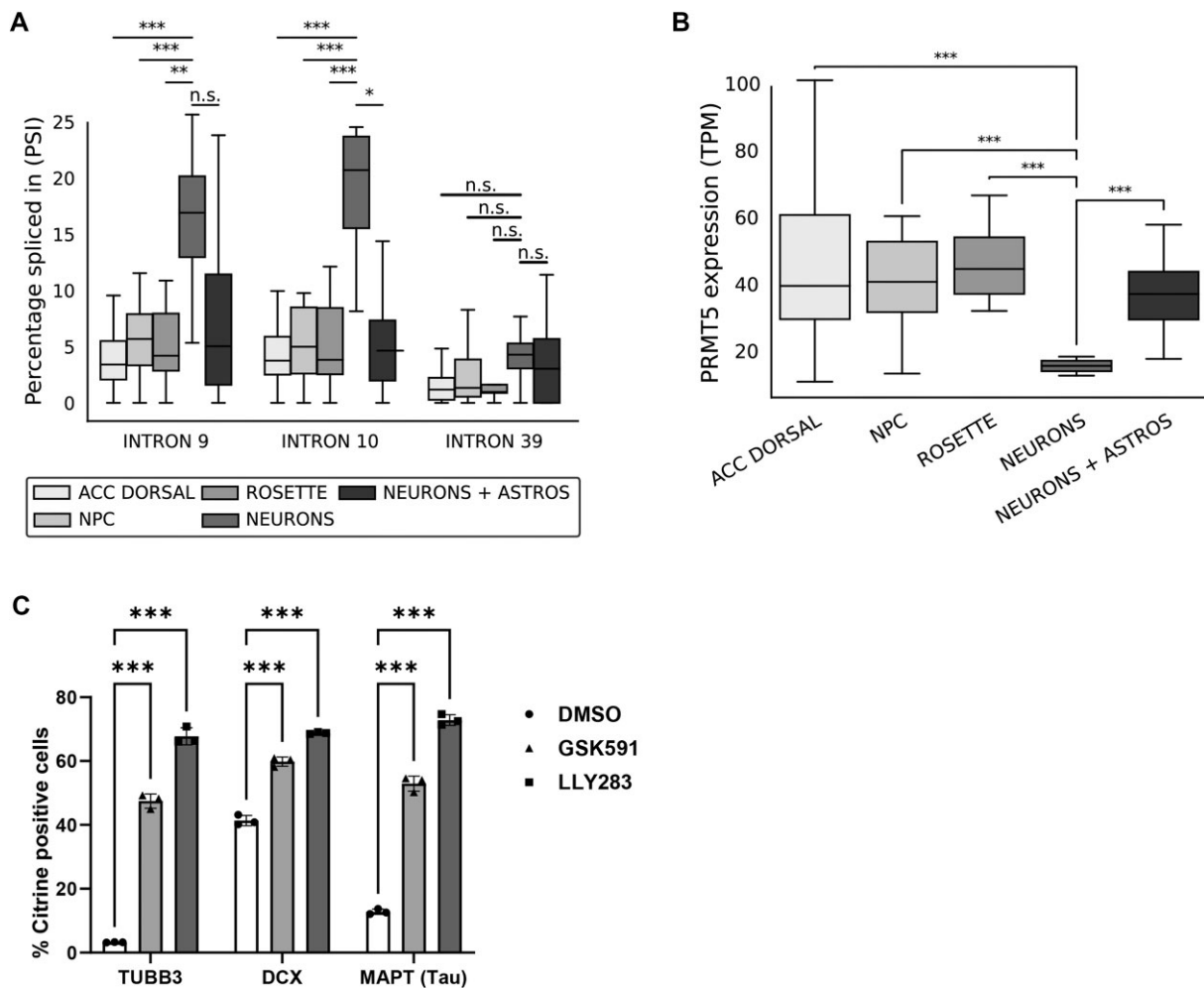


**Figure 6.** Increased expression of truncated, APA *HTT* isoforms correlates with lower PRMT5 levels during neuronal differentiation. **(A)** Boxplot showing the percentage spliced-in (PSI,  $y$ -axis) values for each of the evaluated *HTT* introns ( $x$ -axis) across four distinct stages of neuronal development (early differentiating cells represented as ACC dorsal in white, NPC in light gray, rosettes in medium gray, neurons in gray, and a mixture of neurons plus astrocytes in dark gray). The bars indicate the statistical significance calculated when comparing neurons with other tissues using two-sample independent  $t$ -test with unequal variance, with asterisks indicating a  $P$ -value  $< .05$  and a  $\Delta$ PSI ( $PSI_{\text{neuron}} - PSI_{\text{target}}$ )  $> 10$ . **(B)** Boxplot showing the expression in transcripts per million (TPM,  $y$ -axis) for PRMT5 across the same four different cell types in distinct stages of neuronal development as in panel (A) above. The bars indicate the statistical significance calculated when comparing neurons with other tissues, with asterisks indicating a  $P$ -value  $< .05$  and a  $\log_2$ FoldChange( $\text{Exp}_{\text{Neuron}} / \text{Exp}_{\text{Target}}$ )  $> 1$  or  $< -1$ . **(C)** PRMT5 inhibition in GBM stem cells induces neuronal differentiation. Tubulin  $\beta$ III (TUBB3), Doublecortin (DCX), and MAPT (Tau)-Citrine fluorescence reporter assays in GBM stem cell line G523 showing robust induction of neuronal differentiation after treatment with either 1  $\mu\text{M}$  GSK591 or 1  $\mu\text{M}$  LLY283 for 14 days. Cells were collected and processed by flow cytometry at 14 days of treatment. Data were analyzed using two-way ANOVA. Data are shown as mean  $\pm$  SD;  $n = 3$  biological replicates. Asterisks indicate statistical significance. \*\*\* $P < .001$ , \*\* $P < .01$ , \* $P < .05$ , ns: not significant.

(Fig. 6B) appears to be functionally required for neurogenesis and is further correlated to induction of the truncated APA *HTT* isoform.

## Discussion

Here, we identify PRMT5 inhibition as a novel way to lower *HTT* mRNA and protein levels. This was observed for both full-length WT *HTT* as well as poly-glutamine-expanded *HTT* alleles. The mechanism was mediated by impaired intron splicing, leading to activation of intronic PAS sites and PCPA of the *HTT* transcript.

PRMT5 inhibition has been reported to induce widespread mis-splicing in various cell types. A major splicing subtype affected by loss in PRMT5 activity is intron retentions. Intron retentions can be detrimental for gene expression as they

not only affect mRNA stability by introducing premature stop codons that lower gene and protein expression by NMD, but can also lead to cryptic cleavage of mRNA and activation of PA sites, ultimately resulting in mRNA truncation or novel short isoforms [50, 51]. Here, we identified several novel intronic cryptic PAS in introns 9 and 10 of the *HTT* gene that are activated by PRMT5 inhibition. This results in PCPA of the *HTT* mRNA, which may ultimately lead to a decrease in full-length *HTT* protein levels. This mechanism contrasts with the recently reported splicing inhibitors, which lower *HTT* protein levels by incorporating a novel pseudoexon that introduces premature termination codons, resulting in NMD.

We identified a dramatic activation of a cluster of cryptic intronic PAS sites in introns 9 and 10 of the *HTT* transcript upon PRMT5 inhibition. Although we observed this phenomenon in GBM stem cells and fibroblasts, it is likely conserved in

many other cell types. In support of this notion, the majority of intronic *HTT* PAS sites found in the polyA database (a compendium of experimentally validated PAS sites) [43] map to *HTT* introns 9 and 10, and are identical to the ones found in GBM stem cells and fibroblasts. Moreover, the same *HTT* introns were identified to be highly retained in a transcriptomic study of *HTT* splicing isoforms in post-mortem brains [43]. Notably, the RNA-seq reads in introns 9 and 10 in that study showed highly abundant transcripts nearly equal in depth to that of flanking exons [52]. Additional evidence for transcription in introns 9 and 10 has been documented in GENCODE v21 [53]. Altogether, this evidence points to a novel *HTT* isoform terminating in introns 9 or 10 that is produced by the activation of a cluster of cryptic APA sites in *HTT* introns 9 and 10, leading to premature termination and mRNA truncation. A similar mechanism, termed preT-IR, for premature termination-intron retained mRNAs, was recently described in SFPQ null ALS [51]. Notably, it seems to be prevalent in neuronal mRNAs, and the preT-IR transcripts accumulate in neurites [51].

IPA is a well-documented mechanism of gene expression regulation that can result in either gene/protein downregulation or the creation of truncated proteins with novel 3'UTRs. We investigated the latter possibility by western blot analysis using several HTT antibodies, but were unable to detect any truncated, lower molecular weight HTT protein isoforms enriched in the PRMT5 inhibitor-treated cell lysates. This may be due to low expression levels resulting from RNA turnover mechanisms that cause instability of this isoform, sequestration or retention of the IPA transcript in the nucleus, and/or protein fragment aggregation. Further studies are needed to explore this possibility.

PRMT5 regulates the assembly of the spliceosome by symmetrically dimethylating Smd1, Smd3, and SmB/B' proteins, all of which are snRNP components of the spliceosome. The majority of PRMT5 substrates play a role in RNA processing [54]. The spliceosome machinery interacts with RNA polymerase to enhance transcription speed and elongation rate, particularly across long introns in long genes [46]. Recently, the U1 spliceosome has been reported to control RNA pol II elongation speed and the ability of RNA pol II to elongate through long AT-rich introns [46]. A propensity for slower transcription and weak splicing may result in the activation and utilization of multiple IPA sites as shown previously [55]. We tested whether inhibiting U1 snRNP also induces PCPA in *HTT* mRNA and observed a similar pattern of PAS activation as seen with PRMT5 chemical inhibition. This very much resembles the U1 telescripting model put forward by Dreyfuss and colleagues [44, 45] observed with U1 snRNP inhibition, where proximal intronic PAS sites are being de-repressed [45, 56]. Interestingly, this effect was more evident in long neuronal genes bearing long introns [57], such as *HTT*, and PCPA induction was prevalent in activated neurons, stem cells, and cancer cells [44]. Importantly, neuronal activation caused a transient U1 snRNP shortage, leading to activation of proximal PCPA and transcript shortening [44]. This model fits perfectly with our findings of a transient PRMT5 decrease during neuronal differentiation accompanied by *HTT* mRNA shortening via proximal APA and PCPA induction. It also suggests that PRMT5 inhibition may result in more widespread APA and potential transcriptome shortening via a similar mechanism. In line with this notion, PRMT5 has been reported to directly methylate mRNA cleavage and

PA factors [58] and RNA polymerase elongation factors such as SPT5 as well as the C-terminal domain (CTD) of RNA polymerase II itself [59], thus directly impacting transcription termination. Together, our data support a model where PRMT5 inhibition results in de-repression of proximal intronic PAS sites in the *HTT* gene, similar to U1 snRNP inhibition.

We found that the truncated PAS mRNA levels increase during neuronal differentiation, concomitant with a decrease in PRMT5 levels. Previous studies had also found lower PRMT5 levels during neuronal differentiation that were associated with increased levels of intron retention in neurons [15]. Moreover, this decrease in PRMT5 expression appears to be important for neurogenesis as inhibition of PRMT5 activity potentially induced the neuronal marker tubulin  $\beta$ III (TUBB3) in GBM stem cells. Thus, lower PRMT5 expression/activity in differentiating neurons seems to be a requirement for neuronal differentiation to proceed. This is consistent with previous reports for PRMT5, where higher PRMT5 activity is required in neural stem cells and neural progenitor cells, whereas it decreases in differentiating neurons as well as oligodendrocytes and glial cells [15, 60]. The decrease in PRMT5 expression in neurons was accompanied with increased *HTT* intron retention and proximal APA activation, leading to a truncated *HTT* mRNA isoform and lower HTT protein levels. This suggests that lowering full-length HTT via the production of a truncated isoform is a consequence of lower PRMT5 activity during neuronal differentiation. Although this may seem counterintuitive at first glance for a protein mutated in a neurodegenerative disease, there is evidence showing that HTT is required for neural stem cell division, and lack of HTT promotes neural stem cell differentiation [19]. Further studies will be required to investigate the role of HTT isoforms during neuronal differentiation. The isoform-switching mechanism we uncovered has the advantage of being tightly linked to transient spliceosomal component imbalances, which may be essential for the transition from neuronal stem cells to NPCs and, subsequently to mature neurons [44], and possibly during neuronal regeneration [61]. We believe our findings thus provide important insights into HTT regulation during neuronal development and differentiation.

## Acknowledgements

We would like to thank Paul Boutz and Christian Braun for helpful discussions and sharing data. We thank Magdalena Szewczyk and Shili Duan for help with westerns and tissue culture experiments, respectively, Shamini Ayyadhuri for help with scRNA-seq data and Jean-Philippe Brosseau for help with qPCR primer design. We thank Tamara Maiuri and François Bachand for providing critical input on the manuscript. The graphical abstract and Fig. 5A schematics were created using Created in BioRender. Duan, S. (2025) <https://BioRender.com/jknh0zu>.

*Author contributions:* M.Y.: investigation, methodology, data curation, formal analysis, visualization, validation, writing-original draft, writing-review and editing; M.A.A.: investigation, methodology, formal analysis, data curation, writing-original draft; F.E.C.: formal analysis, software, methodology, visualization, validation, writing-original draft, writing-review and editing; J.C.H.: investigation, methodology, formal analysis; M.I.M. investigation, methodology, formal analysis, writing-review and editing; A.M.S. formal analysis, visualization, software, methodology, data cura-

tion, writing-original draft, writing-review and editing; G.M. investigation, methodology, resources, formal analysis, data curation, visualization, writing-original draft, writing-review and editing; M.A. investigation, resources, methodology; G.B. investigation, resources, methodology; V.T.: formal analysis, methodology; S.H.L.: formal analysis, methodology, supervision; M.S.-O.: formal analysis, visualization, methodology; P.S. investigation, resources, methodology; M.K.: investigation, methodology, resources; L.R.: investigation, methodology, analysis; C.F.B.: investigation, methodology, resources; M.A.P.: supervision, resources; R.K.: investigation, resources; T.P.: supervision, resources, funding acquisition; M.T.: supervision, funding acquisition; S.A.: supervision, resources, funding acquisition; P.B.D. supervision, resources, funding acquisition; G.D.B.: supervision, funding acquisition; R.T.: supervision, funding acquisition, methodology, resources; K.B.M. supervision, data curation, writing-review and editing; D.B.-L.: supervision, methodology; D.S. supervision, funding acquisition, methodology; R.J.H. conceptualization, supervision, resources, methodology, writing-original draft, writing-review and editing; C.H.A.: supervision, resources, funding acquisition, writing-original draft, writing-review and editing; P.P.: conceptualization, resources, supervision, methodology, analysis, validation, writing-original draft, writing-review and editing

## Supplementary data

Supplementary data is available at NAR online.

## Conflict of interest

None declared.

## Funding

M.Y. was funded by a MITACS accelerate fellowship and MiTO2i scholarship. M.A.A. was funded by a Princess Margaret Postdoctoral Fellowship and was funded by a MITACS Accelerate fellowship. This work was supported by Stand Up to Cancer Canada (SU2C-AACR-DT-19-15) provided by the Government of Canada through Genome Canada and the Canadian Institute of Health Research (142434), with supplemental support from the Ontario Institute for Cancer Research through funding provided by the Government of Ontario. Stand Up To Cancer Canada is a program of the Entertainment Industry Foundation Canada. Research funding is administered by the American Association for Cancer Research International-Canada, the scientific partner of SU2C Canada. D.S. was supported by the following grants: NIH/NIGMS R01GM108646 and the Irma T. Hirsch Trust. Funding to pay the Open Access publication charges for this article was provided by Structural Genomics Consortium. The Structural Genomics Consortium is a registered charity (no: 1097737) that receives funds from Bayer AG, Boehringer Ingelheim, Bristol Myers Squibb, Genentech, Genome Canada through Ontario Genomics Institute [OGI-196], EU/EFPIA/OICR/McGill/KTH/Diamond Innovative Medicines Initiative 2 Joint Undertaking [EubOPEN grant 875510], Janssen, Merck KGaA (aka EMD in Canada and US), Pfizer, and Takeda.

## Data availability

The data underlying this article are available in the article and in its online supplementary material. The RNA-seq data files for the three GBM lines treated with GSK591 or SGC2096 have been reported previously [17] and can be accessed at the European Genome-phenome Archive (EGA) under the accession ID EGAS00001004397. The mass spectrometry proteomics data have been also reported previously [17] and deposited to the ProteomeXchange Consortium via the PRIDE partner repository with the dataset identifier PXD021635.

## References

- Bates GP, Dorsey R, Gusella JF *et al.* Huntington disease. *Nat Rev Dis Primers* 2015;1:15005. <https://doi.org/10.1038/nrdp.2015.5>
- Shaw E, Mayer M, Ekwaru P *et al.* Epidemiology and economic burden of Huntington's disease: a Canadian provincial public health system perspective. *J Med Econ* 2022;25:212–9. <https://doi.org/10.1080/13696998.2022.2033493>
- Coppen EM, van der Grond J, Roos RAC. Atrophy of the putamen at time of clinical motor onset in Huntington's disease: a 6-year follow-up study. *J Clin Mov Disord* 2018;5:2. <https://doi.org/10.1186/s40734-018-0069-3>
- Neueder A, Landles C, Ghosh R *et al.* The pathogenic exon 1 HTT protein is produced by incomplete splicing in Huntington's disease patients. *Sci Rep* 2017;7:4408–10. <https://doi.org/10.1038/s41598-017-01510-z>
- Schultz JL, Neema M, Nopoulos PC. Unravelling the role of huntingtin: from neurodevelopment to neurodegeneration. *Brain* 2023;146:4408–10. <https://doi.org/10.1093/brain/awad353>
- Bhattacharyya A, Trotta CR, Narasimhan J *et al.* Small molecule splicing modifiers with systemic HTT-lowering activity. *Nat Commun* 2021;12:7299. <https://doi.org/10.1038/s41467-021-27157-z>
- Keller CG, Shin Y, Monteys AM *et al.* An orally available, brain penetrant, small molecule lowers huntingtin levels by enhancing pseudoexon inclusion. *Nat Commun* 2022;13:1150. <https://doi.org/10.1038/s41467-022-28653-6>
- Krach F, Stemick J, Boerstler T *et al.* An alternative splicing modulator decreases mutant HTT and improves the molecular fingerprint in Huntington's disease patient neurons. *Nat Commun* 2022;13:6797. <https://doi.org/10.1038/s41467-022-34419-x>
- Friesen WJ, Massenet S, Pausshkin S *et al.* SMN, the product of the spinal muscular atrophy gene, binds preferentially to dimethylarginine-containing protein targets. *Mol Cell* 2001;7:1111–7. [https://doi.org/10.1016/S1097-2765\(01\)00244-1](https://doi.org/10.1016/S1097-2765(01)00244-1)
- Meister G, Eggert C, Buhler D *et al.* Methylation of Sm proteins by a complex containing PRMT5 and the putative U snRNP assembly factor pICln. *Curr Biol* 2001;11:1990–4. [https://doi.org/10.1016/S0960-9822\(01\)00592-9](https://doi.org/10.1016/S0960-9822(01)00592-9)
- Paknia E, Chari A, Stark H *et al.* The ribosome cooperates with the assembly chaperone pICln to initiate formation of snRNPs. *Cell Rep* 2016;16:3103–12. <https://doi.org/10.1016/j.celrep.2016.08.047>
- Bezzi M, Teo SX, Muller J *et al.* Regulation of constitutive and alternative splicing by PRMT5 reveals a role for Mdm4 pre-mRNA in sensing defects in the spliceosomal machinery. *Genes Dev* 2013;27:1903–16. <https://doi.org/10.1101/gad.219899.113>
- Ferguson MW, Kennedy CJ, Palpagama TH *et al.* Current and possible future therapeutic options for Huntington's disease. *J Cent Nerv Syst Dis* 2022;14:11795735221092517. <https://doi.org/10.1177/11795735221092517>
- Tabrizi SJ, Estevez-Fraga C, van Roon-Mom WMC *et al.* Potential disease-modifying therapies for Huntington's disease: lessons learned and future opportunities. *Lancet Neurol* 2022;21:645–58. [https://doi.org/10.1016/S1474-4422\(22\)00121-1](https://doi.org/10.1016/S1474-4422(22)00121-1)

15. Braun CJ, Stanciu M, Boutz PL *et al.* Coordinated splicing of regulatory detained introns within oncogenic transcripts creates an exploitable vulnerability in malignant glioma. *Cancer Cell* 2017;32:411–26. <https://doi.org/10.1016/j.ccell.2017.08.018>
16. Maron MI, Casill AD, Gupta V *et al.* Type I and II PRMTs inversely regulate post-transcriptional intron detention through Sm and CHTOP methylation. *eLife* 2022;11:e72867. <https://doi.org/10.7554/eLife.72867>
17. Sachamitr P, Ho JC, Ciamponi FE *et al.* PRMT5 inhibition disrupts splicing and stemness in glioblastoma. *Nat Commun* 2021;12:979. <https://doi.org/10.1038/s41467-021-21204-5>
18. Szewczyk MM, Luciani GM, Vu V *et al.* PRMT5 regulates ATF4 transcript splicing and oxidative stress response. *Redox Biol* 2022;51:102282. <https://doi.org/10.1016/j.redox.2022.102282>
19. Conforti P, Camnasio S, Mutti C *et al.* Lack of huntingtin promotes neural stem cells differentiation into glial cells while neurons expressing huntingtin with expanded polyglutamine tracts undergo cell death. *Neurobiol Dis* 2013;50:160–70. <https://doi.org/10.1016/j.nbd.2012.10.015>
20. Lopes C, Aubert S, Bourgois-Rocha F *et al.* Dominant-negative effects of adult-onset huntingtin mutations alter the division of human embryonic stem cells-derived neural cells. *PLoS One* 2016;11:e0148680. <https://doi.org/10.1371/journal.pone.0148680>
21. Furlanis E, Scheiffele P. Regulation of neuronal differentiation, function, and plasticity by alternative splicing. *Annu Rev Cell Dev Biol* 2018;34:451–69. <https://doi.org/10.1146/annurev-cellbio-100617-062826>
22. Han H, Best AJ, Braunschweig U *et al.* Systematic exploration of dynamic splicing networks reveals conserved multistage regulators of neurogenesis. *Mol Cell* 2022;82:2982–99. <https://doi.org/10.1016/j.molcel.2022.06.036>
23. Mauger O, Lemoine F, Scheiffele P. Targeted intron retention and excision for rapid gene regulation in response to neuronal activity. *Neuron* 2016;92:1266–78. <https://doi.org/10.1016/j.neuron.2016.11.032>
24. Mazille M, Buczak K, Scheiffele P *et al.* Stimulus-specific remodeling of the neuronal transcriptome through nuclear intron-retaining transcripts. *EMBO J* 2022;41:e110192. <https://doi.org/10.15252/embj.2021110192>
25. Traummuller L, Gomez AM, Nguyen TM *et al.* Control of neuronal synapse specification by a highly dedicated alternative splicing program. *Science* 2016;352:982–6. <https://doi.org/10.1126/science.aaf2397>
26. McKeever PM, Sababi AM, Sharma R *et al.* Single-nucleus multiomic atlas of frontal cortex in amyotrophic lateral sclerosis with a deep learning-based decoding of alternative polyadenylation mechanisms. *bioRxiv*, <https://doi.org/10.1101/2023.12.22.573083>, 23 December 2023, preprint: not peer reviewed.
27. Hung CL, Maiuri T, Bowie LE *et al.* A patient-derived cellular model for Huntington's disease reveals phenotypes at clinically relevant CAG lengths. *MBoC* 2018;29:2809–20. <https://doi.org/10.1091/mbc.E18-09-0590>
28. Kelly JJ, Stechishin O, Chojnacki A *et al.* Proliferation of human glioblastoma stem cells occurs independently of exogenous mitogens. *Stem Cells* 2009;27:1722–33. <https://doi.org/10.1002/stem.98>
29. Caron NS, Anderson C, Black HF *et al.* Reliable resolution of full-length huntingtin alleles by quantitative immunoblotting. *J Huntingtons Dis* 2021;10:355–65. <https://doi.org/10.3233/JHD-200463>
30. Cuddleston WH, Fan X, Sloofman L *et al.* Spatiotemporal and genetic regulation of A-to-I editing throughout human brain development. *Cell Rep* 2022;41:111585. <https://doi.org/10.1016/j.celrep.2022.111585>
31. van de Leemput J, Boles NC, Kiehl TR *et al.* CORTECON: a temporal transcriptome analysis of *in vitro* human cerebral cortex development from human embryonic stem cells. *Neuron* 2014;83:51–68. <https://doi.org/10.1016/j.neuron.2014.05.013>
32. Luisier R, Tyzack GE, Hall CE *et al.* Intron retention and nuclear loss of SFPQ are molecular hallmarks of ALS. *Nat Commun* 2018;9:2010.
33. Ooi J, Langley SR, Xu X *et al.* Unbiased profiling of isogenic Huntington disease hPSC-derived CNS and peripheral cells reveals strong cell-type specificity of CAG length effects. *Cell Rep* 2019;26:2494–508. <https://doi.org/10.1016/j.celrep.2019.02.008>
34. Tano V, Utami KH, Yusof N *et al.* Widespread dysregulation of mRNA splicing implicates RNA processing in the development and progression of Huntington's disease. *EBioMedicine* 2023;94:104720. <https://doi.org/10.1016/j.ebiom.2023.104720>
35. Love MI, Huber W, Anders S. Moderated estimation of fold change and dispersion for RNA-seq data with DESeq2. *Genome Biol* 2014;15:550. <https://doi.org/10.1186/s13059-014-0550-8>
36. Hartley SW, Mullikin JC. Detection and visualization of differential splicing in RNA-seq data with JunctionSeq. *Nucleic Acids Res* 2016;44:e127.
37. Li WV, Zheng D, Wang R *et al.* MAAPER: model-based analysis of alternative polyadenylation using 3' end-linked reads. *Genome Biol* 2021;22:222. <https://doi.org/10.1186/s13059-021-02429-5>
38. Navickas A, Asgharian H, Winkler J *et al.* An mRNA processing pathway suppresses metastasis by governing translational control from the nucleus. *Nat Cell Biol* 2023;25:892–903. <https://doi.org/10.1038/s41556-023-01141-9>
39. Scheer S, Ackloo S, Medina TS *et al.* A chemical biology toolbox to study protein methyltransferases and epigenetic signaling. *Nat Commun* 2019;10:19. <https://doi.org/10.1038/s41467-018-07905-4>
40. Bonday ZQ, Cortez GS, Grogan MJ *et al.* LLY-283, a potent and selective inhibitor of arginine methyltransferase 5, PRMT5, with antitumor activity. *ACS Med Chem Lett* 2018;9:612–7. <https://doi.org/10.1021/acsmchemlett.8b00014>
41. Marques RE, Guabiraba R, Russo RC *et al.* Targeting CCL5 in inflammation. *Expert Opin Ther Targets* 2013;17:1439–60. <https://doi.org/10.1517/14728222.2013.837886>
42. Jenal M, Elkon R, Loayza-Puch F *et al.* The poly(A)-binding protein nuclear 1 suppresses alternative cleavage and polyadenylation sites. *Cell* 2012;149:538–53. <https://doi.org/10.1016/j.cell.2012.03.022>
43. Wang R, Zheng D, Yehia G *et al.* A compendium of conserved cleavage and polyadenylation events in mammalian genes. *Genome Res* 2018;28:1427–41. <https://doi.org/10.1101/gr.237826.118>
44. Berg MG, Singh LN, Younis I *et al.* U1 snRNP determines mRNA length and regulates isoform expression. *Cell* 2012;150:53–64. <https://doi.org/10.1016/j.cell.2012.05.029>
45. Kaida D, Berg MG, Younis I *et al.* U1 snRNP protects pre-mRNAs from premature cleavage and polyadenylation. *Nature* 2010;468:664–8. <https://doi.org/10.1038/nature09479>
46. Mimoso CA, Adelman K. U1 snRNP increases RNA pol II elongation rate to enable synthesis of long genes. *Mol Cell* 2023;83:1264–79. <https://doi.org/10.1016/j.molcel.2023.03.002>
47. Tapial J, Ha KCH, Sterne-Weiler T *et al.* An atlas of alternative splicing profiles and functional associations reveals new regulatory programs and genes that simultaneously express multiple major isoforms. *Genome Res* 2017;27:1759–68. <https://doi.org/10.1101/gr.220962.117>
48. Petric Howe M, Crerar H, Neeves J *et al.* Physiological intron retaining transcripts in the cytoplasm abound during human motor neurogenesis. *Genome Res* 2022;32:1808–25.
49. Terryn J, Tricot T, Gajjar M *et al.* Recent advances in lineage differentiation from stem cells: hurdles and opportunities? *F1000Res* 2018;7:220. <https://doi.org/10.12688/f1000research.12596.1>
50. Grabski DF, Broseus L, Kumari B *et al.* Intron retention and its impact on gene expression and protein diversity: a review and a practical guide. *Wiley Interdiscip Rev RNA* 2021;12:e1631. <https://doi.org/10.1002/wrna.1631>

51. Taylor R, Hamid F, Fielding T *et al.* Prematurely terminated intron-retaining mRNAs invade axons in SFPQ null-driven neurodegeneration and are a hallmark of ALS. *Nat Commun* 2022;13:6994. <https://doi.org/10.1038/s41467-022-34331-4>
52. Labadorf AT, Myers RH. Evidence of extensive alternative splicing in post mortem human brain HTT transcription by mRNA sequencing. *PLoS One* 2015;10:e0141298. <https://doi.org/10.1371/journal.pone.0141298>
53. Harrow J, Frankish A, Gonzalez JM *et al.* GENCODE: the reference human genome annotation for The ENCODE Project. *Genome Res* 2012;22:1760–74. <https://doi.org/10.1101/gr.135350.111>
54. Maron MI, Lehman SM, Gayatri S *et al.* Independent transcriptomic and proteomic regulation by type I and II protein arginine methyltransferases. *iScience* 2021;24:102971. <https://doi.org/10.1016/j.isci.2021.102971>
55. Tian B, Pan Z, Lee JY. Widespread mRNA polyadenylation events in introns indicate dynamic interplay between polyadenylation and splicing. *Genome Res* 2007;17:156–65. <https://doi.org/10.1101/gr.5532707>
56. Venters CC, Oh JM, Di C *et al.* U1 snRNP telescripting: suppression of premature transcription termination in introns as a new layer of gene regulation. *Cold Spring Harb Perspect Biol* 2019;11:a032235. <https://doi.org/10.1101/cshperspect.a032235>
57. Oh JM, Di C, Venters CC *et al.* U1 snRNP telescripting regulates a size-function-stratified human genome. *Nat Struct Mol Biol* 2017;24:993–9. <https://doi.org/10.1038/nsmb.3473>
58. Boisvert FM, Cote J, Boulanger MC *et al.* A proteomic analysis of arginine-methylated protein complexes. *Mol Cell Proteomics* 2003;2:1319–30. <https://doi.org/10.1074/mcp.M300088-MCP200>
59. Zhao DY, Gish G, Braunschweig U *et al.* SMN and symmetric arginine dimethylation of RNA polymerase II C-terminal domain control termination. *Nature* 2016;529:48–53. <https://doi.org/10.1038/nature16469>
60. Calabretta S, Vogel G, Yu Z *et al.* Loss of PRMT5 promotes PDGFR $\alpha$  degradation during oligodendrocyte differentiation and myelination. *Dev Cell* 2018;46:426–40. <https://doi.org/10.1016/j.devcel.2018.06.025>
61. Poplawski GHD, Kawaguchi R, Van Niekerk E *et al.* Injured adult neurons regress to an embryonic transcriptional growth state. *Nature* 2020;581:77–82. <https://doi.org/10.1038/s41586-020-2200-5>
62. Katz Y, Wang ET, Siltterra J *et al.* Quantitative visualization of alternative exon expression from RNA-seq data. *Bioinformatics* 2015;31:2400–2. <https://doi.org/10.1093/bioinformatics/btv034>